ACS APPLIED MATERIALS & INTERFACES

Research Article

www.acsami.org

Biocompatible and Highly Luminescent Near-Infrared $CuInS_2/ZnS$ Quantum Dots Embedded Silica Beads for Cancer Cell Imaging

Mohamed F. Foda, Liang Huang, Feng Shao, and He-You Han*

State Key Laboratory of Agricultural Microbiology, College of Science, Huazhong Agricultural University, Wuhan 430070, China

Supporting Information

ABSTRACT: Bright and stable $CuInS_2/ZnS@SiO_2$ nanoparticles with near-infrared (NIR) emission were competently prepared by incorporating the as-prepared hydrophobic $CuInS_2/ZnS$ quantum dots (QDs) directly into lipophilic silane micelles and subsequently an exterior silica shell was formed. The obtained $CuInS_2/ZnS@SiO_2$ nanoparticles homogeneously comprised both single-core and multicore remarkable $CuInS_2/ZnS$ QDs, while the silica shell thickness could be controlled to within 5−10 nm and their overall size was 17−25 nm. Also, the functionalized $CuInS_2/ZnS$ QDs encapsulated in the silica spheres, expedited their bioconjugation with holo-Transferrin (Tf) for further cancer cell imaging. The $CuInS_2/ZnS@SiO_2$ nanoparticles not only showed a dominant NIR band-edge luminescence at 650−720 nm with a quantum yield (QY) between 30 and 50%, without a recognized photoluminescence (PL) red shift, but also exhibited excellent PL and colloidal stability in aqueous media. Impressively, the cytotoxicity studies revealed minor suppression on cell viability under both $CuInS_2/ZnS@SiO_2$ and $CuInS_2/ZnS@SiO_2$@Tf concentrations up to 1 mg/mL. The application in live-cell imaging revealed that the potential of $CuInS_2/ZnS$ QDs as biocompatible, robust, cadmium-free, and brilliant NIR emitters is considered promising for fluorescent labels.

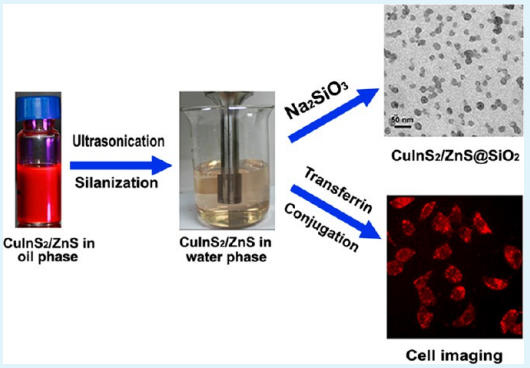

KEYWORDS: *$CuInS_2/ZnS@SiO_2$, NIR QDs, lipophilic silane micelles, cytotoxicity, fluorescent labels, cadmium-free*

1. INTRODUCTION

To date, quantum dots (QDs) have grasped much more attention, in comparison with organic dyes especially in bioimaging fields, because of the enrollment of QDs as a novel class of materials with unique optical and electronic properties, such as remarkable quantum yield (QY), size-tunable photoluminescence (PL), symmetrical and sharp emission peaks, multicolor fluorescence under a single-wavelength excitation source, and high photobleaching resistance.[1,2] Despite all previous motivations that favor the use of QDs for biomedical imaging, until now it remains severely restricted for possible in vivo applications because most available QDs are composed of known toxic elements such as Cd, Hg, Pb, Se, Te, As, etc. Exemplify reports have emphasized the eventual release of heavy elements on the cellular membrane casing biodegradation in the cellular environment and affecting the osmotic equilibrium of the cell, which effectively increases the cytotoxicity effect of these QDs.[3] Therefore, the safety of QD biological labels maintains a major obstacle in their future biomedical exploration.

The I−III−VI_2 QD synthetic research as a rapidly emerging discipline, with intentionally well-controlled structure and multifunctional properties, indicates their potential as novel biolabeling agents.[4,5] At this point, I−III−VI_2 $CuInS_2$ QDs are environmentally friendly and biocompatible because they contain no heavy metal ions. More encouragingly, the narrow band gap of this semiconductor allows their emission to be tunable from a visible to near-infrared (NIR) optical window by tailoring the nanocrystal size. This feature enables $CuInS_2$ QDs to have more sufficient optical penetration in biological tissue from the NIR optical window of 650−900 nm,[6] compared with the traditional II−VI QDs.

Similar to the well-developed II−VI QDs, the I−III−VI_2 QDs with well-controlled shape, size, and composition are commonly synthesized via a thermal decomposition route in organic solvents under elevated temperature.[7,8] Unfortunately, they are incompatible with the physiological environment. Therefore, a phase transfer from oil to water is inevitable to ensure the water solubility of the I−III−VI_2 QDs before further biological applications. Moreover, the fluorescent labels for biomedical imaging should possess several qualities including good photochemical stability, excellent water solubility, and controlled particle size, which should be small enough to avoid possible accumulation in the body and to enhance the transportation ability in cells.[9,10] In the past few years, several techniques such as silica coating,[11] ligand exchange,[12] and amphiphilic polymer encapsulation[13] have been promoted to make hydrophobic nanoparticles water-soluble. Among these

Received: November 12, 2013
Accepted: January 16, 2014
Published: January 16, 2014

techniques, the silica shell worked as a unique capsule for the QDs, which was advantageous in terms of being nontoxic, chemically inert, and optically transparent. Moreover, compared with ligand exchange and polymer encapsulation, the silica surface can be easily modified and the silica shell can protect the inner nanoparticles from environmental damage especially chemical etching and oxidation.[14]

Traditional silica coating methods could be categorized into Stöber and reverse microemulsion approaches, which mainly depend on the exchange of QD original ligands by the silane such as (3-mercaptopropyl)trimethoxysilane[14−16] or partially hydrolyzed tetraethyl orthosilicate (TEOS) in the reverse microemulsion approach.[17,18] Unlikely, rarely have silica coatings been applied on the $CuInS_2$-based QDs in traditional ways, probably because of the existence of a strong coordinating ligand, 1-dodecanethiol (DDT), which proves to be critical in balancing the reactivity of copper (Cu) and indium (In) precursors forming homogeneous ternary components of the nanocrystals.[10] Previous reports have shown that the foreign coordinating thiols were unable to replace DDT easily in a phase-transfer process of $CuInS_2$ QDs[10] and the DDT-capped CdTe QDs showed no incorporation in silica spheres by the reverse microemulsion method.[18] Apparently, the previously reported coating mechanism does not fit for the $CuInS_2$ QDs, and to the best of our knowledge, no successful silica coating on $CuInS_2$ QDs has been achieved. Very recently, Xue's group employed a cationic surfactant, namely, cetyltrimethylammonium bromide, to transfer lipophilic zinc-doped $AgInS_2$ QDs into water followed by micelle-templated silica shell growth,[19] showing an aggregated silica/micelle on the outer silica surface, and the generated mesoporous silica shell had difficulty preventing the diffusion of small molecules such as oxygen to degrade the QD surface quality.

Herein, we prepared highly emissive ZnS-passivated $CuInS_2$ QDs in the 650−720 nm emitting region with QY between 30 and 50%, respectively, in the organic phase. To make water dispersible and brilliant $CuInS_2$/ZnS QDs ready for biomedical use, we adopted lipophilic silane encapsulation to incorporate adjustable amounts of hydrophobic $CuInS_2$/ZnS QDs directly into silica beads with a relatively small diameter of around 17−25 nm, which is illustrated in Scheme 1. The silica coating layer maintained the emission properties of QDs regarding the PL spectrum and QY. The obtained $CuInS_2$/ZnS@SiO_2 nanoparticles exhibited advanced stability and low cytotoxicity under cell culture conditions. After surface modification and bioconjugation with holo-Transferrin (Tf), to enhance the bioavailability, the $CuInS_2$/ZnS@SiO_2 particles were successfully recognized by HeLa cells for fluorescent imaging.

Scheme 1. Schematic Illustration of the Silica Coating Procedures for Single-Core Hydrophobic $CuInS_2$/ZnS QDs

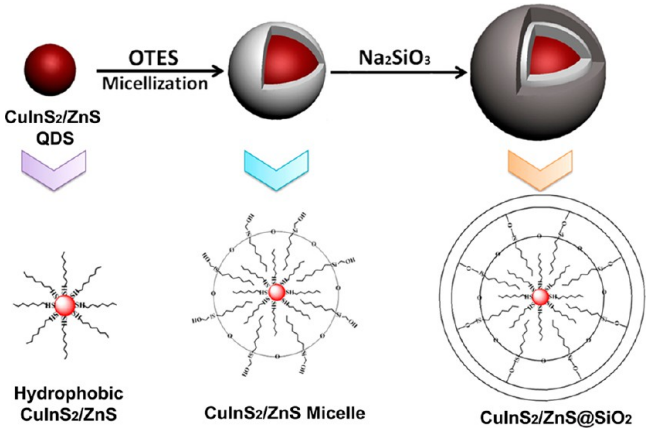

2. RESULTS AND DISCUSSION

We adopted the surfactant-free emulsification of lipophilic silane (*n*-octyltriethoxysilane, OTES) in a water−ammonia solution, assisted by ultrasonication, to prepare silane-encapsulated QD micelles. To achieve this, the hydrophobic $CuInS_2$/ZnS QDs were dissolved in OTES, and this silane precursor was shattered into small oil droplets under cavitation, forming an oil-in-water microemulsion, as is clearly presented in Figure 1A. The ammonia addressed in this step proved to be crucial in transforming the silane emulsion droplets into water-soluble micelles, during catalysis of alkylsiloxane into amphiphilic alkylsilanetriol, which served properly as a surfactant.[22] The microemulsion became more transparent after it had been sonicated for 30 min because more alkylsilanetriols were produced, which favored a smaller emulsion droplet size (Figure 1B). The final microemulsion after 1 h of sonication appeared totally transparent (Figure 1C), indicating a small individual size of $CuInS_2$/ZnS@OTES micelles. To prevent possible coalescence of newly formed QD micelles, sodium silicate was introduced to deposit a thin silica layer on the silanol anchor points, forming colloidally stable $CuInS_2$/ZnS@SiO_2 nanostructures.

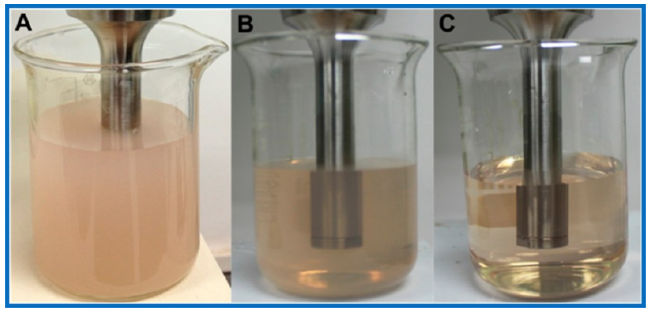

Figure 1. Appearance of $CuInS_2$/ZnS@OTES micelles in water with ultrasonication times of (A) 0 min, (B) 30 min, and (C) 60 min followed by filtration.

The as-prepared $CuInS_2$/ZnS QD from the organic phase has an average diameter of 2−4 nm, as illustrated in Figure 2A. The good dispersity of the $CuInS_2$/ZnS QDs in nonpolar solvents facilitated the subsequent formation of small-sized $CuInS_2$/ZnS@SiO_2 nanoparticles. The X-ray diffraction (XRD) pattern in Figure S1 in the Supporting Information (SI) demonstrated the core/shell structure of the $CuInS_2$/ZnS QDs, where the diffraction peaks of $CuInS_2$/ZnS QDs were located between those of $CuInS_2$ and ZnS. The successful surface passivation of the ZnS shell consequently isolated the $CuInS_2$ core from the environmental solution, improving the photochemical stability of the QDs. Parts B and C of Figure 2 clearly reveal the transmission electron microscopy (TEM) image of the $CuInS_2$/ZnS@SiO_2 nanoparticles with isotropic silica growth, indicating the formation of silica layers around the micelles and localization of $CuInS_2$/ZnS QDs in the center of each silica nanobead. The average diameter as well as the QD loading amount of each $CuInS_2$/ZnS@SiO_2 bead, as shown in Figure 2B,C, can be finely tuned by adjusting the amount of $CuInS_2$/ZnS QDs taken from the organic phase, achieving final

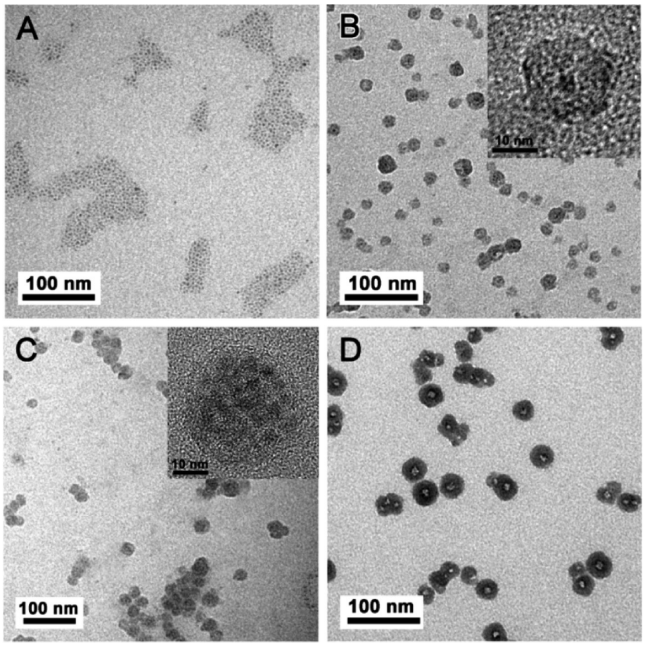

Figure 2. TEM images of the $CuInS_2/ZnS$ QDs dispersed in chloroform (A) and $CuInS_2/ZnS@SiO_2$ nanoparticles with 17 nm. Inset: HRTEM image of a single center $CuInS_2/ZnS$ QD embedded into one silica nanobead (B) and 25 nm diameter. Inset: HRTEM image of a multicore $CuInS_2/ZnS$ QD embedded into one silica nanobead (C) and $CuInS_2/ZnS@SiO_2$ nanoparticles after Stöber growth from parts B–D. (D) Successful formation of a 5–10-nm-thick silica shell after TEOS condensation.

sizes of 17 and 25 nm, respectively. Furthermore, elemental analysis by energy-dispersive X-ray (EDX) proved the composition of the addressed material, as shown in Figure S2 in the SI. The observed peaks could be well attributed to the compositing elements from $CuInS_2/ZnS$ QDs as well as the silica shell [the nickel signal is from the nickel (Ni) TEM grind as used]. Extensive silica coating was further carried out to control the growth of the silica shell using the Stöber method, which employs alcohol, ammonia, and TEOS.[23] In order to demonstrate the controlled silica growth, the as-prepared $CuInS_2/ZnS@SiO_2$ nanoparticles were dispersed in the Stöber system. Figure 2D displays $CuInS_2/ZnS@SiO_2$ after TEOS hydroxylation and condensation, forming an extensive silica shell of 5–10 nm. After this procedure, the core/shell structure of $CuInS_2/ZnS@SiO_2$ was clearly observed, indicating a brighter region in the center, namely, the organosilica core, which has lower electron density than the outer silica shell. The obtained result demonstrates that the desirable overgrowth of the silica shell can be conducted in a controllable way. In subsequent work, we used the $CuInS_2/ZnS@SiO_2$ nanoparticles without extensive silica coating. In comparison with recent reports about water-soluble ternary QDs such as $CuInS_2/ZnS$ and $AgInS_2/ZnS$, the current $CuInS_2/ZnS@SiO_2$ structure is advantageous in dimensional and morphological control including (a) smaller size verified from 17 to 25 nm in contrast to polymer (such as chitosan)-encapsulated $CuInS_2/ZnS$ QDs,[20] (b) a multicore structure, which is brighter than the silica spheres containing a single QD or limited QDs,[19,24,25] and (c) direct emulsification of lipophilic silane in water by ultrasonication that skipped the use of surfactant for phase transfer, which would induce mesoporous silica shell formation.[19,26]

The properties of QDs are the most important features for their potential applications. The single-core- and multicore-structured $CuInS_2/ZnS@SiO_2$ nanoparticles with a fluorescence emission peak at 650 nm showed nearly identical spectra of both UV–vis absorption and PL, as demonstrated in Figure S3 in the SI. This indicated that the structural difference of $CuInS_2/ZnS@SiO_2$ nanoparticles has little influence on their optical performance. We further prepared two different kinds of $CuInS_2/ZnS$ QDs with fluorescence emission peaks at 650 and 720 nm, respectively, whose UV–vis absorption and PL spectra are shown in Figure S4 in the SI. The PL spectrum of $CuInS_2/ZnS@SiO_2$ was nearly the same as that of the oil-soluble QDs with 650 nm wavelength (Figure 3A), exhibiting a relatively high QY of 50% (compared with a QY of 65% in the organic phase), which clarifies that the silica coating layer maintained the emission properties of QDs regarding the PL spectrum and QY. For the NIR $CuInS_2/ZnS$ with a 720 nm emission wavelength and a QY of 42%, the coating strategy was also successfully carried out, showing identically matched PL peaks with the hydrophobic QDs as well as a QY of 31% after silica coating, as presented in Figure 3B. The highly preserved QY

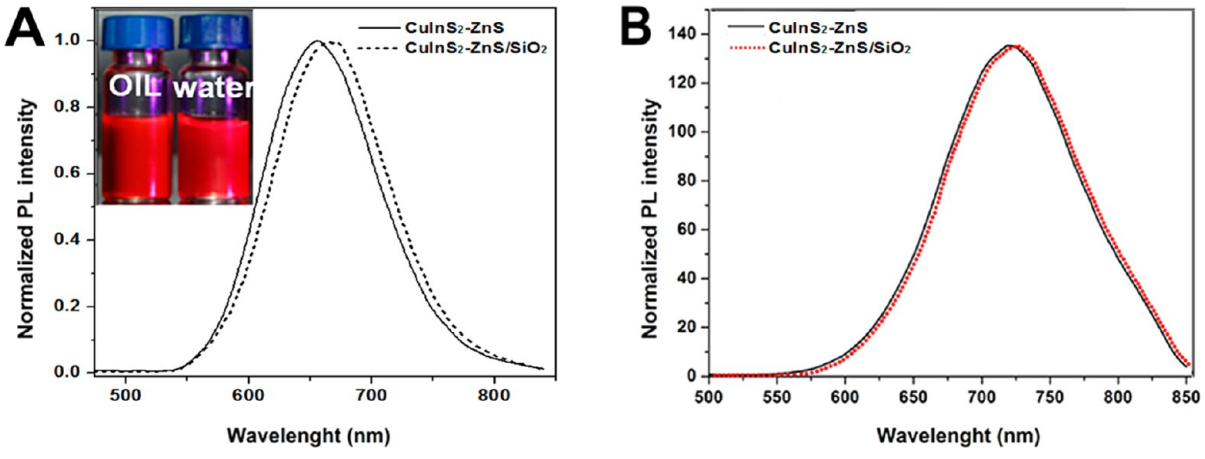

Figure 3. (A) PL QY spectra of $CuInS_2/ZnS$ QDs and $CuInS_2/ZnS@SiO_2$ with an emission wavelength of 650 nm and a QY of 50%. Inset: photographs of $CuInS_2/ZnS$ QDs in the oil phase and $CuInS_2/ZnS@SiO_2$ in the water phase under UV light. (B) PL QY spectra of $CuInS_2/ZnS$ QDs and $CuInS_2/ZnS@SiO_2$ with an emission wavelength of 720 nm and a QY of 31%.

and spectral features (without an obvious PL red shift from hydrophobic QDs as previously observed[19,25]) probably benefited from lipophilic saline encapsulation (hydrophobic interaction) on $CuInS_2/ZnS$ QDs without disturbing the originally capping ligands. This favored the surface passivation of $CuInS_2/ZnS$ QDs, which is critical for their optical emission properties.

To access the colloidal stability and biocompatibility of the obtained $CuInS_2/ZnS@SiO_2$ nanoparticles for biological applications, dynamic light scattering (DLS) was performed to monitor the particle hydrodynamic diameter at periodic time intervals during 24 h. The temperature was set to 37 °C during the whole experiment, and deionized (DI) water, phosphate-buffered saline (PBS), and Dulbecco's modified eagle medium (DMEM) solutions were used as the culture media. As displayed in Figure 4, the hydrodynamic diameters of the

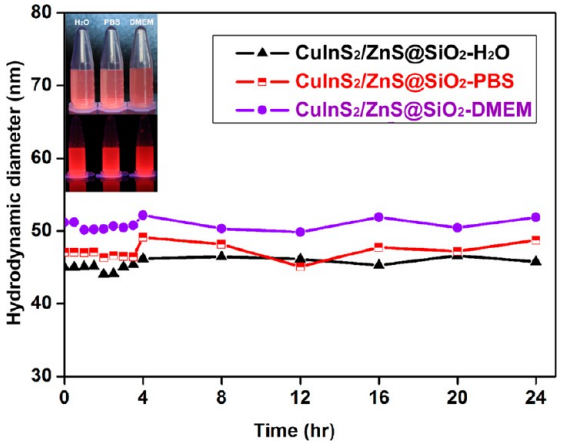

Figure 4. Hydrodynamic diameters of $CuInS_2/ZnS@SiO_2$ nanoparticles in DI water, PBS, and DMEM incubated at 37 °C. Inset: digital photographs of $CuInS_2/ZnS@SiO_2$ in different media under room light (upper) and UV light (lower).

$CuInS_2/ZnS@SiO_2$ nanoparticles in the three media appear to be larger compared with their dry size from TEM observation, which possibly originated from the existence of an electrostatic bilayer in water. The $CuInS_2/ZnS$ QDs incorporating silica nanoparticles in DI water, PBS, and DMEM media all exhibited stable hydrodynamic diameters, indicating that no aggregation occurred during 24 h of incubation. This improved colloidal stability in aqueous solution could be attributed to the stable cross-linked silica layer around the lipophilic saline encapsulated $CuInS_2/ZnS$ QDs, which effectively protected the QDs from aggregation in a biological medium.

To illustrate the ability of as-prepared $CuInS_2/ZnS@SiO_2$ nanoparticles in potential biological imaging, we adopted holo-Transferrin (Tf), one kind of well-studied ligand protein for targeted cancer cell imaging and drug delivery,[12,28,29] to functionalize the nanoparticle surface. To achieve conjugation of the desired protein with $CuInS_2/ZnS@SiO_2$, we first grafted the silica surface by epoxy groups using (3-glycidyloxypropyl)-trimethoxysilane (GPTMS)−silane coupling in organic solvents. A covalent bond between the epoxy group and protein amino group was subsequently formed in a basic solution. Fourier transform infrared (FT-IR) spectrometry was performed to investigate the protein functionalization process of $CuInS_2/ZnS@SiO_2$. Figure S5 in the SI demonstrates featured bands at 1646, 1534, and 3418 cm^{-1} from $CuInS_2/ZnS@SiO_2$@Tf compared with $CuInS_2/ZnS@SiO_2$, which could be attributed to the characteristic bands of the amino group ($-NH_2$) from conjugated protein. This indicates the successful functionalization of $CuInS_2/ZnS@SiO_2$ nanoparticles with Tf. DLS was further employed to characterize the protein-conjugated nanoparticles. The hydrodynamic diameter of $CuInS_2/ZnS@SiO_2$@Tf was 54 nm, which was about 10 nm larger than the original $CuInS_2/ZnS@SiO_2$ of 43 nm (Figure S6 in the SI), possibly because of the existence of protein molecules around the silica surface. The size distribution histogram, together with the photographs of $CuInS_2/ZnS@SiO_2$ and $CuInS_2/ZnS@SiO_2$@Tf, indicates the good dispersion ability and fluorescence of the addressed materials.

The cytotoxicity of this new type of $CuInS_2/ZnS@SiO_2$ and functionalized $CuInS_2/ZnS@SiO_2$ with Tf nanoparticles, which is of most concern before their biological applications, was evaluated by MTT assay with various particle concentrations. As depicted in Figure 5A, along with the increased concentrations of $CuInS_2/ZnS@SiO_2$ and $CuInS_2/ZnS@SiO_2$@Tf, the cell viabilities all remained at high levels, and no obvious suppression was observed, especially for $CuInS_2/ZnS@SiO_2$@Tf. At a concentration of 1 mg/mL, the cell viability after 24 h of incubation was approximately 100%. Notably, this concentration is much higher than that used for cellular staining with QD conjugates diluted in blood circulation under in vivo conditions.[27] Furthermore, we performed a photostability test of $CuInS_2/ZnS@SiO_2$ in a cell culture medium. As shown in Figure 5B, no PL intensity decrease was observed during 1 h of successive excitations, indicating that the silica shell and hydrophobic bilayers robustly protected the $CuInS_2/ZnS$ QDs emitting character. The preliminary results demonstrated that the obtained $CuInS_2/ZnS@SiO_2$ and $CuInS_2/ZnS@SiO_2$@Tf nanoparticles are qualified for future biological labeling.

The Tf-functionalized $CuInS_2/ZnS@SiO_2$ was further applied to target HeLa cells, which overexpress Tf receptors on their surface. As shown in Figure 5C, the HeLa cells incubated with $CuInS_2/ZnS@SiO_2$@Tf nanoparticles for 12 h emitted a clear red color under UV excitation, indicating effective interaction of these nanoparticles with HeLa cells. Control experiments were carried out on HeLa cells and the HEK 293 cell line using $CuInS_2/ZnS@SiO_2$ and $CuInS_2/ZnS@SiO_2$@Tf, respectively, as presented in Figure S7 in the SI. A low fluorescent signal was observed while incubating $CuInS_2/ZnS@SiO_2$ with the HeLa cells (Figure S7A in the SI), and no fluorescent signal was detected after incubation of $CuInS_2/ZnS@SiO_2$@Tf with HEK 293 cells, which have limited Tf receptors compared with HeLa cells (Figure S7B in the SI). These results clarified qualification of this new type of core/shell-structured $CuInS_2/ZnS@SiO_2$ nanoparticles with red-to-NIR emission in targeted cellular imaging.

3. CONCLUSION

In summary, novel and high-performance $CuInS_2/ZnS$ QDs incorporating silica "micelle" nanoparticles with high QY and dominant band-edge NIR emission at 650−720 nm were prepared. The $CuInS_2/ZnS$ QDs with variable amounts could be embedded into silica beads with final sizes of 17−25 nm and a controllable silica shell, which could be biofunctionalized for further cell imaging applications. Remarkably, the silanized $CuInS_2/ZnS$ QDs well retained their original optical properties, achieving a high QY of 30−50% and excellent photostability and colloidal stability in aqueous media. The cytotoxicity and

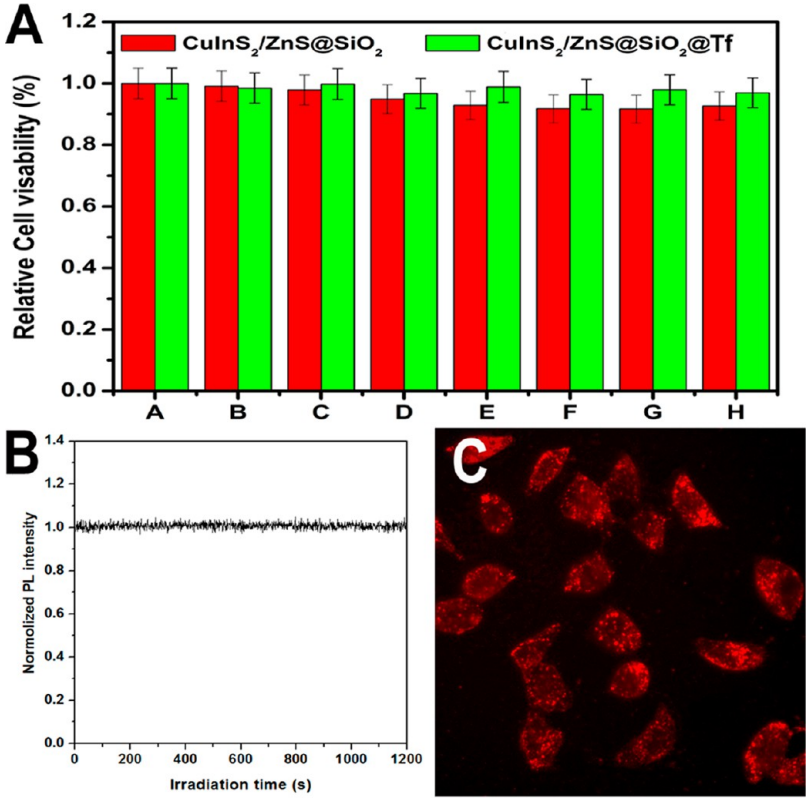

Figure 5. (A) Cytotoxicity studies of $CuInS_2/ZnS@SiO_2$ and $CuInS_2/ZnS@SiO_2$@Tf nanoparticles by MTT assay on HeLa cells after 24 h of incubation. (B) PL intensity of $CuInS_2/ZnS@SiO_2$ nanoparticles in DMEM during 1 h of excitation. (C) Fluorescent image of HeLa cells incubated with $CuInS_2/ZnS@SiO_2$@Tf nanoparticles under UV excitation.

cell imaging studies encouragingly indicated that the $CuInS_2/ZnS@SiO_2$ nanoparticles are promising red-to-NIR fluorescent labels with good biocompatibility and bright and robust NIR emission.

4. EXPERIMENTAL SECTION

4.1. Chemicals. Copper acetate [$Cu(Ac)_2$, 99.99%], indium acetate [$In(Ac)_3$, 99.99%], zinc acetate [$Zn(Ac)_2$, 99.99%], 1-dodecanethiol (DDT; 98%), 1-octadecene (ODE; 90%), oleic acid (OA; 90%), oleylamine (OAm; 97%), sodium silicate solution (27 wt % SiO_2), and tetraethyl orthosilicate (TEOS; 99%) were purchased from Aldrich. *N*-Octyltriethoxysilane (OTES; 98%) was purchased from TCI. Chloroform, methanol, ethanol, and an aqueous ammonia solution (28%) were supplied by Sinopharm Chemical Reagent Co., Ltd. 3-(4,5-Dimethylthiazol-2-yl)-2,5-diphenyltetrazolium bromide (MTT; Aldrich), dimethyl sulfoxide (DMSO; Sinopharm), streptomycin, trypsin, and ethylenediaminetetraacetic acid were all commercially available. Dulbecco's modified eagle medium (DMEM) was purchased from Sino-American Biotechnology Company. Cells were obtained from Cell Bank of Chinese Academy of Sciences (CBCAS). All chemicals were used without further purification. The water used through all experiments had an 18.2 MΩ·cm resistivity.

4.2. Synthesis of Colloidal $CuInS_2$ and $CuInS_2/ZnS$ Core/Shell QDs. The $CuInS_2$ nanoparticles were synthesized according to the reported procedure with some modifications.[20] In a typical core synthesis, the initial three precursors $Cu(Ac)_2$ (0.2 mmol), $In(Ac)_3$ (0.2 mmol), and 2.0 mL (8.35 mmol) of DDT (as the sulfur precursor) were introduced in a 25 mL three-neck flask along with the addition of 3 mL of ODE and 0.3 mL of OA. Then the mixture was gently stirred for 15 min under a N_2 flow at 160 °C until the preferable solution was obtained. Afterward, the reaction temperature was raised to 230 °C, and the solution was retained at this temperature to allow for growth of $CuInS_2$ core QDs. Through the synthesis process, a progressive color change in the reaction solution was observed from slight yellow to yellow, orange, red, and finally crimson, indicating subsequent nucleation growth of $CuInS_2$ core QDs. Several samples were taken at different time intervals and injected into chloroform to terminate QD growth for UV−vis absorbance and PL measurements without any size sorting. The preparation of the zinc precursor solution was attempted by dissolving 2 mmol of $Zn(Ac)_2$ in ODE/OAm (its ratio was 4:1.4, in all 5.4 mL) at 140 °C under a N_2 flow for 7−10 min. The ZnS coating was accomplished after confirmation of the growth of the $CuInS_2$ core QDs; as the temperature was lowered to 190 °C to adjust the environment for the addition of the ZnS precursor, gentle injection was performed within 5 min, and then the temperature was raised again to 230 °C for 30 min for subsequent growth of a ZnS shell. Heating was stopped immediately after the expected time (30 min) was reached, and then the solution was left to cool to room temperature; an equal volume of chloroform was added thereafter. The resulting $CuInS_2/ZnS$ core/shell QDs were isolated by precipitation using a mixture of organic solvents (anhydrous methanol/acetone) ratio (1:4); more importantly, this step was repeated several times to ensure total removal of the oil phase, which will be a main obstacle in the aqueous transfer process, centrifuging and decanting the supernatant. The residues were redispersed into 10 mL of chloroform or toluene.

4.3. Silica Coating of $CuInS_2/ZnS$ QDs. The coating was achieved in a stepwise fashion by silanization with lipophilic silane followed by sodium silicate deposition in water. Briefly, 500 μL of $CuInS_2/ZnS$ was precipitated using a 1:4 anhydrous methanol/acetone mixture. The supernatant was discarded, and the residue organic solvent in wet precipitate was evaporated by an air flow. The precipitate was then dissolved by 20 μL of OTES using the sonicator to facilitate solubilization. Then 20 mL of water was added along with 30 μL of $NH_3·H_2O$, and the mixture was processed by a tapered microtip sonicator (VCX800 Ultrasonic processor, Sonics) with a 1-cm-diameter probe and 20% amplitude. Over a period of 1 h, a working circle consisting of 5 s of sonication and 3 s of pausing was designed. The resulting solution was passed through a 0.22-μm-pore-

dx.doi.org/10.1021/am4050772 | ACS Appl. Mater. Interfaces 2014, 6, 2011−2017

size filter to remove any existing cloudiness. A total of 0.8 mL of a 0.54 wt % sodium silicate aqueous solution was added to the solution with continuous stirring for 36 h. Finally, the crude solution of silica beads was purified by circles of ultrafiltration using a 30 kDa MWCO filter to reach an optical density of 0.1 at 570 nm.

4.4. Characterization of $CuInS_2/ZnS@SiO_2$ Core/Shell Nanoparticles. TEM images were acquired on a JEM-2010FEF transmission electron microscope. High-resolution TEM (HRTEM) was taken on a JEM-2100F field-emission electron microscope (made in Japan). XRD patterns were taken on a Rigaku D/MAX-RB diffractometer with Cu Kα radiation (λ = 0.15406 nm). EDX was carried out on a JEOL JEM-2100F 136-5 instrument with an active area of 30 mm^2. UV−vis absorption spectra were recorded on Nicolet Evolution 300 UV−vis spectrometer. The PL spectrum was measured on an Edinburgh FLS920 spectrometer. FT-IR spectra were measured on a Nicolet Avatar-330 spectrometer with 4 cm^{-1} resolution using the KBr pellet technique. The PL stability was tested on a Perkin-Elmer LS-55 spectrometer in time drive mode. The particle colloidal stability in DI water, PBS (10 mM, pH 7.4), and DMEM was measured by DLS. Furthermore, Rhodamine 6G in an ethanol solution was used as a standard for calculating the PL QY before and after silica coating conducted on $CuInS_2/ZnS$ QDs, according to the described procedure.[21]

4.5. Functionalization of $CuInS_2/ZnS@SiO_2$ Nanoparticles. To conjugate $CuInS_2/ZnS@SiO_2$ nanoparticles with Tf, the silica surface was preliminarily modified with GPTMS. Approximately 20 μL of the concentrated $CuInS_2/ZnS@SiO_2$ nanoparticles were dissolved in 2 mL of ethanol and 20 μL of GPTMS. The mixture was allowed to continue stirring under 25 °C for 12 h, and the $CuInS_2/ZnS@SiO_2$ particles were collected by high-speed centrifugation (13000 rpm) for 15 min. The obtained particles were washed several times with ethanol to ensure removal of excess GPTMS. The purified $CuInS_2/ZnS@SiO_2$ particles were suspended in 2 mL of PBS followed by the addition of 250 μL of a holo-Tf stock solution with a concentration of 1 mg/mL. After stirring at 25 °C for 12 h, the final particles were purified by centrifugation several times and suspended in a DMEM medium ready for cell culture.

4.6. Cytotoxicity of $CuInS_2/ZnS@SiO_2$ Core/Shell Nanocrystals. For MTT assay, cells were cultured in 96-well plates and incubated for 24 h before experiments until cell growth reached about 80% confluence. $CuInS_2/ZnS@SiO_2$ samples dispersed in DMEM at different concentrations were added to each well to achieve a final concentration of 200 μL/well. Cells were then incubated in these media containing $CuInS_2/ZnS@SiO_2$ at 37 °C and in a 5% CO_2 atmosphere for another 24 h. After incubation, all wells were washed with PBS to remove excess $CuInS_2/ZnS@SiO_2$ and placed in a fresh solution of 200 μL before the next experiments. Afterward, 20 μL MTT stock solutions (5 mg/mL) were added to each well, and cells were then incubated for 4 h at 37 °C. The supernatant was discarded, 150 μL/well of DMSO was added to dissolve the produced formazan, and the plates were shaken for an additional 10 min. The absorbance of purple formazan was recorded at 570 nm.

4.7. Cell Culture and Cell Imaging. Human cervical carcinoma cell line HeLa cells (obtained from CBCAS) was cultured in DMEM supplemented with 10% heat-inactivated fetal bovine serum and antibiotics (100 mg/mL streptomycin and 100 U/mL penicillin) at 37 °C in a humidified atmosphere with 5% CO_2. For the preparation of fluorescent imaging, cells were grown in 6-well plates at a density of 3 × 10^5 per well and took 2 days to reach the desired cells. Under the hood, 20 μL of $CuInS_2/ZnS@SiO_2$@Tf, suspended in a DMEM medium, was added to the cultural medium. The cells were incubated with a nanoparticle solution for 12 h. After incubation, the DMEM medium was taken out and washed three times with PBS. The stained cells were imaged by an inverted fluorescence microscope (Nikon Eclipse Ti series). All of the obtained images were captured under UV excitation.

■ ASSOCIATED CONTENT

Supporting Information

XRD patterns of $CuInS_2$ QDs (red) and $CuInS_2/ZnS$ QDs (black), EDX of the $CuInS_2/ZnS@SiO_2$ nanoparticles, UV−vis absorption and PL spectra of the two types of $CuInS_2/ZnS@SiO_2$, UV−vis absorption (red) and PL (blue) spectra for oil-soluble $CuInS_2/ZnS$ QDs with 650 and 750 nm emission, FT-IR spectra of $CuInS_2/ZnS@SiO_2$ and $CuInS_2/ZnS@SiO_2$@Tf nanoparticles, DLS histograms of $CuInS_2/ZnS@SiO_2$ and $CuInS_2/ZnS@SiO_2$@Tf with insets showing digital photographs of the addressed material in PBS under UV light, and control experiments of HeLa cells incubated with $CuInS_2/ZnS@SiO_2$ nanoparticles for 12 h and the HEK 293 cell line incubated with $CuInS_2/ZnS@SiO_2$@Tf for 12 h. This material is available free of charge via the Internet at http://pubs.acs.org.

■ AUTHOR INFORMATION

Corresponding Author

*Phone: +(86) 027-87288246. Fax: +(86) 027-87288246. E-mail: hyhan@mail.hzau.edu.cn.

Notes

The authors declare no competing financial interest.

■ ACKNOWLEDGMENTS

We gratefully appreciate funding support for this research from the National Natural Science Foundation of China (Grant 21175051, 21375043), the Natural Science Foundation of Hubei Province Innovation Team (Grant 2011CDA115), and the Fundamental Research Funds for the Central Universities (Grant 2012SC04, 2013SC17).

■ REFERENCES

(1) Medintz, I. L.; Uyeda, H. T.; Goldman, E. R.; Mattoussi, H. *Nat. Mater.* **2005**, *4*, 435−446.
(2) Resch-Genger, U.; Grabolle, M.; Cavaliere-Jaricot, S.; Nitschke, R.; Nann, T. *Nat. Methods* **2008**, *5*, 763−775.
(3) Lewinski, N.; Colvin, V.; Drezek, R. *Small* **2008**, *4*, 26−49.
(4) Li, L.; Daou, T. J.; Texier, I.; Kim Chi, T. T.; Liem, N. Q.; Reiss, P. *Chem. Mater.* **2009**, *21*, 2422−2429.
(5) Pons, T.; Pic, E.; Lequeux, N.; Cassette, E.; Bezdetnaya, L.; Guillemin, F.; Marchal, F.; Dubertret, B. *ACS Nano* **2010**, *4*, 2531−2538.
(6) Smith, A. M.; Mancini, M. C.; Nie, S. *Nat. Nanotechnol.* **2009**, *4*, 710−711.
(7) Zhong, H.; Zhou, Y.; Ye, M.; He, Y.; Ye, J.; He, C.; Yang, C.; Li, Y. *Chem. Mater.* **2008**, *20*, 6434−6443.
(8) Xie, R.; Rutherford, M.; Peng, X. *J. Am. Chem. Soc.* **2009**, *131*, 5691−5697.
(9) Chen, F.; Gerion, D. *Nano Lett.* **2004**, *4*, 1827−1832.
(10) Wang, Y.; Chen, J.; Irudayaraj, J. *ACS Nano* **2011**, *5*, 9718−9725.
(11) Bruchez, M.; Moronne, M.; Gin, P.; Weiss, S.; Alivisatos, A. P. *Science* **1998**, *281*, 2013−2016.
(12) Chan, W. C.; Nie, S. *Science* **1998**, *281*, 2016−2018.
(13) Pellegrino, T.; Manna, L.; Kudera, S.; Liedl, T.; Koktysh, D.; Rogach, A. L.; Keller, S.; Rädler, J.; Natile, G.; Parak, W. J. *Nano Lett.* **2004**, *4*, 703−707.
(14) Gerion, D.; Pinaud, F.; Williams, S. C.; Parak, W. J.; Zanchet, D.; Weiss, S.; Alivisatos, A. P. *J. Phys. Chem., B* **2001**, *105*, 8861−8871.
(15) Nann, T.; Mulvaney, P. *Angew. Chem., Int. Ed.* **2004**, *43*, 5393−5396.
(16) Jana, N. R.; Earhart, C.; Ying, J. Y. *Chem. Mater.* **2007**, *19*, 5074−5082.
(17) Darbandi, M.; Thomann, R.; Nann, T. *Chem. Mater.* **2005**, *17*, 5720−5725.

(18) Koole, R.; van Schooneveld, M. M.; Hilhorst, J.; de Mello Donegá, C.; Hart, D. C.; van Blaaderen, A.; Vanmaekelbergh, D.; Meijerink, A. *Chem. Mater.* **2008**, *20*, 2503−2512.
(19) Sheng, Y.; Tang, X.; Xue, J. *J. Mater. Chem.* **2012**, *22*, 1290−1296.
(20) Deng, D.; Chen, Y.; Cao, J.; Tian, J.; Qian, Z.; Achilefu, S.; Gu, Y. *Chem. Mater.* **2012**, *24*, 3029−3037.
(21) Qu, L.; Peng, X. *J. Am. Chem. Soc.* **2002**, *124*, 2049−2055.
(22) Huang, L.; Luo, Z.; Han, H. *Chem. Commun.* **2012**, *48*, 6145−6147.
(23) Stöber, W.; Fink, A.; Bohn, E. *J. Colloid Interface Sci.* **1968**, *26*, 62−69.
(24) Wang, M.; Liu, X.; Cao, C.; Wang, L. *J. Mater. Chem.* **2012**, *22*, 21979−21986.
(25) Hsu, J.-C.; Huang, C.-C.; Ou, K.-L.; Lu, N.; Mai, F.-D.; Chen, J.-K.; Chang, J.-Y. *J. Mater. Chem.* **2011**, *21* (48), 19257−19266.
(26) Hu, X.; Zrazhevskiy, P.; Gao, X. *Ann. Biomed. Eng.* **2009**, *37*, 1960−1966.
(27) Michalet, X.; Pinaud, F.; Bentolila, L.; Tsay, J.; Doose, S.; Li, J.; Sundaresan, G.; Wu, A.; Gambhir, S.; Weiss, S. *Science* **2005**, *307*, 538−544.
(28) Tekle, C.; Deurs, B. v.; Sandvig, K.; Iversen, T.-G. *Nano Lett.* **2008**, *8*, 1858−1865.
(29) Wang, J.; Tian, S.; Petros, R. A.; Napier, M. E.; DeSimone, J. M. *J. Am. Chem. Soc.* **2010**, *132*, 11306−11313.